Inorganic Chemistry

pubs.acs.org/IC Article

Synthesis, Characterization, and Biological Activity of Hybrid Thiosemicarbazone−Alkylthiocarbamate Metal Complexes

Sarah A. Andres,[§] Kritika Bajaj,[§] Nicholas S. Vishnosky,[§] Megan A. Peterson, Mark S. Mashuta, Robert M. Buchanan,* Paula J. Bates,* and Craig A. Grapperhaus*

Cite This: https://dx.doi.org/10.1021/acs.inorgchem.0c00182 Read Online

ACCESS | Metrics & More | Article Recommendations | Supporting Information

ABSTRACT: A series of hybrid ligands (H_2L^1−H_2L^3) derived from 4-methyl-3-thiosemicarbazide and hydrazinecarbothioic acid *O*-alkyl esters were synthesized and characterized by NMR. The ligands were chelated with copper (**4**−**6**), nickel (**7**−**9**), and zinc (**10**−**12**) and characterized by spectroscopy, electrochemistry, and single crystal X-ray crystallography. The chelated metals displayed substantial anodic shifts in the $Cu^{II/I}$ reduction potential of ∼160 mV relative to their bis(thiosemicarbazone) analogues. The metal chelates **4**−**12** were evaluated for potential anticancer activity by MTT assays, and selected results were confirmed by clonogenic and trypan blue assays. The copper derivatives **4** and **6** were found to have potent and cancer-selective antiproliferative effects, with GI_{50} values less than 100 nM in A549 lung adenocarcinoma cells compared with at least 20-fold less activity in IMR90 nonmalignant lung fibroblasts. In comparison, the nickel complexes were much less active and had little cancer-selectivity. Varying by ligand, the zinc complexes were less potent or had comparable activity compared to that of the corresponding copper complex. UV−visible spectroscopy indicated that zinc complex **10** was transmetalated in the presence of equimolar copper, whereas nickel complex **7** was not. Copper complexes **4** and **6** were also assessed in the NCI60 screen and were found to have cytotoxic activity against most solid tumor cell lines. In MTT assays, **4** and **6** were substantially more active against A549 cancer cells than Cu(ATSM) and were more cancer-selective (for A549 compared to IMR-90) than Cu(GTSM). Our results suggest that hybrid thiosemicarbazone−alkylthiocarbamate copper complexes have potential for development as new anticancer agents.

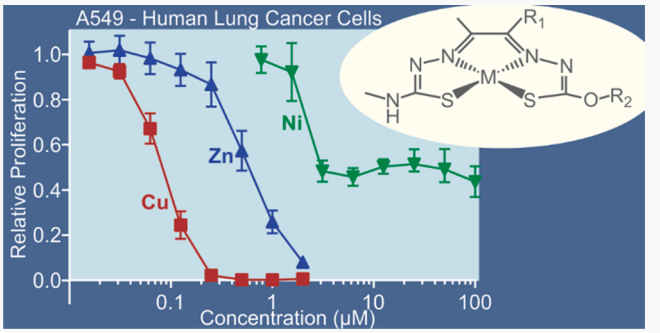

INTRODUCTION

Common treatments for cancer include surgery, hormone therapy, radiation, immunotherapy, targeted therapy, and chemotherapy.[1] However, current methods are often inadequate and about 35% of those with cancer will die because of it (i.e., over 600,000 people/year in the United States), usually within five years of diagnosis.[1] Furthermore, due to their lack of selectivity for cancer cells compared to healthy cells, many current anticancer drugs can cause serious (sometimes life-threatening) side effects. New agents that are more effective at killing aggressive cancer cells while sparing healthy cells are an area of intense interest.

Recently, the imaging[2−10] and therapeutic[7,11−20] applications of various bis(thiosemicarbazone) (BTSC) copper complexes have been extensively studied. The BTSC structure (Scheme 1) can be readily modified through changes in the substituents on the ligand backbone and on the pendent amine, making them good candidates for structure activity relationship (SAR) studies. Antitumor activity of glyoxal bis(thiosemicarbazone) was first reported more than 60 years ago.[21] Subsequent work showed excellent antitumor activity against a number of transplanted rodent tumors with 3-ethoxy-2-oxobutyraldehyde bis(thiosemicarbazone), H_2KTS.[22−24] It was recognized at that time that the activities of these BTSC ligands were likely due to metal chelation, and later studies confirmed that the copper chelate was the active species.[22,24−27] However, toxicity concerns appear to have prevented Cu(KTS) from progressing to clinical trials.[28] Currently, the two most studied Cu(BTSC) complexes are Cu(ATSM) and Cu(GTSM). While Cu(ATSM) is being explored as a diagnostic imaging tool[2−7] and a treatment for neurodegenerative diseases,[16,17,20] Cu(GTSM) is being studied as a potential anticancer and antimicrobial agent.[12,14,29,30] The key difference of these two complexes lies in the ligand backbone where the methyl substituents of Cu(ATSM) are replaced with hydrogen atoms in Cu(GTSM). This affects the $Cu^{II/I}$ reduction potential, with Cu(GTSM) being reduced at

Received: January 17, 2020

Scheme 1. Comparison of Metal Bis(Thiosemicarbazone), Metal Bis(Alkylthiocarbamate), and Hybrid Metal Thiosemicarbazone−Alkylthiocarbamate Structures

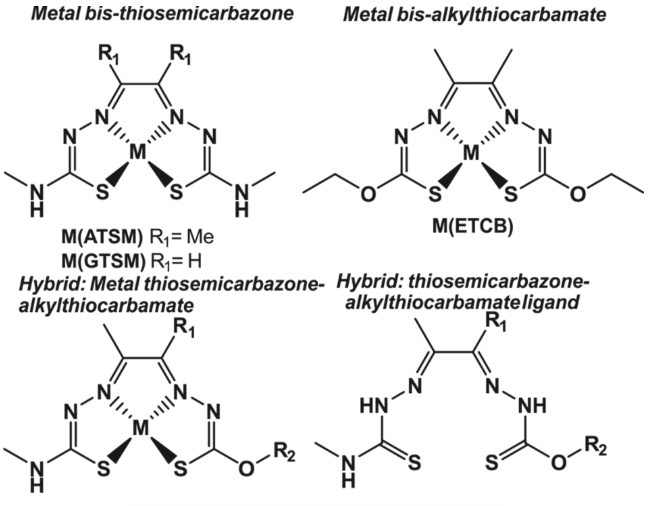

R_1	R_2	M	Ligand
Me	Et	Cu(**4**), Ni(**7**), Zn(**10**)	H_2L^1 (**1**)
Me	n-Pr	Cu(**5**), Ni(**8**), Zn(**11**)	H_2L^2 (**2**)
Ph	Et	Cu(**6**), Ni(**9**), Zn(**12**)	H_2L^3 (**3**)

potentials 160 mV more anodic than Cu(ATSM).[12] The difference in the biological activity of these two complexes has been attributed to this difference in reduction potential.[12] Many other copper complexes have demonstrated potential for *in vivo* imaging or therapy,[2,4,31,32] and a few have progressed to human clinical trials, as described in recent reviews.[8,14,15,33−35]

Despite the many examples of biologically active copper complexes, their mechanism of action is not well understood. A commonly proposed mechanism is that the various ligands act as ionophores that carry copper into the cell and release it in the presence of intracellular reductants such as glutathione, thus increasing the intracellular copper concentrations to toxic levels.[8,14,15,33−35] The presence and redox-cycling of copper can be toxic to cells by multiple mechanisms including induction of reactive oxygen species (ROS), proteasome inhibition, transmetalation of proteins, and damage to proteins, membranes, mitochondria, or DNA.[8,14,15,33−35] In a few cases, specific molecular targets, such as NPL4 segregase adaptor[36] and FDX1 mitochondrial reductase[37] have been identified. The lack of detailed understanding about how most copper complexes work, along with their generally poor solubility and potential for toxicity, are among the likely reasons why copper complexes are not yet in wide clinical use.

Consequently, there is significant interest in developing new copper-ATSM/GTSM analogues that might have improved potential as anticancer agents and also in determining how varying physical or chemical properties can influence biological activities. In addition to changes of diamine backbone substituents, a well-developed strategy to modulate the activity of Cu(BTSC) complexes is variation of the pendent amine functional group. Recently, we prepared derivatives of BTSC with pendent alkoxides in place of pendent amine groups (Scheme 1).[38] A series of bis(alkylthiocarbamate) Cu complexes were previously prepared with similar structural parameters as those of Cu(BTSC) complexes but with altered electrochemical properties.[38] In the current study, we report the synthesis and characterization of hybrid thiosemicarbazone−alkylthiocarbamate ligands and their Ni, Cu, and Zn complexes (Scheme 1) and evaluate their antiproliferative effects. These hybrid complexes offer an alternate motif to tune the electrochemical properties and activity of BTSC-like complexes. Given the relevance of structure−activity relationships in BTSC complexes, this initial report of these hybrid complexes focuses on their antiproliferative activity and cancer-selectivity.

EXPERIMENTAL SECTION

Materials and Methods. All reagents were obtained from commercially available sources and were used as received unless otherwise noted. Diacetyl-2-(4-*N*-methyl-3-thiosemicarbazone),[32] 1-phenyl-2-propanone-1-(4-*N*-methyl-3-thiosemicarbazone), hydrazinecarbothioic acid *O*-ethyl ester,[39] and hydrazinecarbothioic acid *O*-ethyl ester[39] were prepared using previously reported methods. The glyoxal(bisthiosemicarbazone) (H_2GTSM) was synthesized using modification of the previously known procedure.[40] Solvents were dried and purified using an MBraun solvent purification system. The complexes in this study are air and water stable as solids and were handled on the benchtop with no required protection from the atmosphere.

H_2L^1 (1). Diacetyl-2-(4-*N*-methyl-3-thiosemicarbazone) (1.00 g, 5.77 mmol) was suspended in ethanol (25 mL), and hydrazinecarbothioic acid *O*-ethyl ester (0.69 g, 5.8 mmol) was added. A catalytic amount (6 drops) of concentrated sulfuric acid was added, resulting in a white precipitate. The solid was isolated by filtration and washed with water then ethanol. Yield = 1.35 g (85%). ^{1}H NMR (DMSO-d_6, 500 MHz): δ 1.28 (t, 3H), 2.11 and 2.17 (br, 6H), 3.00 (d, 3H), 4.5(q, 2H), 8.35 (s, 1H), 10.21 (s, 1H), 11.31 and 11.62 (s, 1H). ^{13}C NMR (DMSO-d_6, 400 MHz): δ 11.6, 12.4, 14.4, 31.5, 66.2, 67.3, 148.1, 152.2, 153.8, 178.8, 186.9, 189.0. IR cm^{-1}: 3382, 3253, 1541, 1494 (NH), 2991 and 1411 (CH), 1304 and 1217 (CN), 1130 (CO), 1053 (CS). Elemental analysis calcd for $C_9H_{17}S_2ON_5$: C, 39.25; H, 6.22; N, 25.43. Found: C, 39.12; H, 6.16; N, 25.54.

H_2L^2 (2). Compound $\mathbf{H_2L^2}$ was prepared using the method for $\mathbf{H_2L^1}$. The addition of hydrazinecarbothioic acid *O*-propyl ester (0.77 g, 5.8 mmol) to diacetyl-2-(4-*N*-methyl-3-thiosemicarbazone) (1.00 g, 5.77 mmol) in ethanol (30 mL) yielded a white solid. Yield = 1.50 g (90%). ^{1}H NMR (DMSO-d_6, 500 MHz): δ 0.94 (t, 3H) 1.68 (m, 2H), 2.11 and 2.19 (s/br, 6H), 3.00 (d, 3H), 4.41 (q, 2H), 8.36 (s, 1H), 10.25 (s, 1H), 11.35 and 11.63 (s, 1H). ^{13}C NMR (DMSO-d_6, 400 MHz): δ 10.5, 11.5, 12.3, 21.9, 31.5, 71.5, 72.7, 148.1, 152.1, 153.8, 178.8, 186.8, 189.1. IR cm^{-1}: 3382, 3231, 1540, 1497 (NH), 2968 and 1411 (CH), 1303 and 1211 (CN), 1132 (CO), 1068 (CS). Elemental analysis calcd for $C_{10}H_{19}S_2ON_5$: C, 41.50; H, 6.62; N, 24.20. Found: C, 41.31; H, 6.46; N, 24.02.

H_2L^3 (3). Compound $\mathbf{H_2L^3}$ was prepared using the method described for $\mathbf{H_2L^1}$. The addition of hydrazinecarbothioic acid *O*-ethyl ester (0.43 g, 3.6 mmol) to 1-phenyl-2-propanone-1-(4-*N*-methyl-3-thiosemicarbazone) (0.840 g, 3.6 mmol) in ethanol (25 mL) yielded a white solid. Yield = 0.871 g (72%). ^{1}H NMR (DMSO-d_6, 500 MHz): δ 1.32 (br, 3H), 2.06/2.27(s, 3H), 2.79/2,93 (s, 3H), 4.55 (br, 2H), 6.96−8.31 (5H), 10.21 (s, 1H), 10.77 (s, 1H), 11.87/12.14 (s, 1H). ^{13}C NMR (DMSO-d_6, 400 MHz): δ 12.4,14.3, 17.5, 30.8, 31.4, 61.41, 127.5, 129.3,130.2, 135.4, 143.6, 148.8, 151.54, 179.4, 185.9, 189.0. IR cm^{-1}: 3336, 3223, 1476, 1542 (NH), 2937 and 1417 (CH), 1301 and 1219 (CN), 1195 (CO), 1081 (CS). Elemental analysis calcd for $C_{14}H_{19}S_2ON_5$: C, 49.83; H, 5.67; N, 20.75. Found: C, 49.14; H, 5.60; N, 20.18.

H_2GTSM. H_2GTSM was prepared by dissolving glyoxal (40% aq soln) (3.81 g, 65.65 mmol) in 45 mL of deionized water. To this, 4-methyl-3-thiosemicarbazide (5.524 g, 131.3 mmol) was added. A catalytic amount of concentrated sulfuric acid was added, resulting in a tan precipitate. The solution was left to stir overnight. The solid was isolated by filtration and washed with water. Yield = 5.96 g (98%). ^{1}H NMR (DMSO-d_6, 500 MHz): δ 2.96 (d, 6H), 7.72 (s, 2H), 8.48 (m, 2H), 11.74 (s, 2H). ^{13}C NMR (DMSO-d_6, 400 MHz): δ 31.20,

https://dx.doi.org/10.1021/acs.inorgchem.0c00182
Inorg. Chem. XXXX, XXX, XXX−XXX

140.34, 177.81. IR cm^{-1}: 3305, 1539, 1508 (NH), 3140, 2994, 1416 (CH), 1239 (CN), 1080 (CS).

CuL^1 (4). Compound H_2L^1 (0.354 g, 1.29 mmol) was suspended in methanol (25 mL). To this suspension, copper(II) acetate monohydrate (0.285 g, 1.43 mmol) was added with stirring, giving a red-brown precipitate. The suspension was refluxed with stirring for 4 h and then cooled to room temperature. The solid was then filtered and washed with methanol. Yield = 0.220 g (51%). IR cm^{-1}: 3305 and 1561 (NH), 2937 and 1439 (CH), 1382 and 1217 (CN), 1132 (CO), 1025 (CS), 846 (CuS), 782 (CuN). UV−vis spectrum in acetonitrile (nm) (M^{-1} cm^{-1}): 248 (16,000), 309 (20,000), shoulder around 346 (11,000), 473 (5,100). EPR $g_{||}$ = 2.091, $g_{\perp}$ = 2.061, g_{avg} = 2.071. Elemental analysis calcd for $C_9H_{15}S_2ON_5Cu$: C, 32.08; H, 4.49; N, 20.79. Found: C, 31.53; H, 4.34; N, 20.26 Mass spectrum calcd for $CuL^1 + H^+$: 337.01. Found: 337.01.

CuL^2 (5). Complex **5** was prepared using the same method as described for **4** from H_2L^2 (0.373 g, 1.29 mmol) and copper(II) acetate monohydrate (0.285 g, 1.43 mmol) in methanol (25 mL). Complex **5** was isolated as a red-brown solid. Yield = 0.200 g (44%). IR cm^{-1}: 3329 and 1562 (NH), 2972 and 1465 (CH), 1382 and 1219 (CN), 1019 (CO), 974 (CS), 872 (CuS), 758 (CuN). UV−vis spectrum in acetonitrile (nm) (M^{-1} cm^{-1}): 249 (13,000), 310 (17,000), shoulder around 346 (8,700), 477 (4,300). EPR $g_{||}$ = 2.116 and $g_{\perp}$ = 2.030, g_{avg} = 2.059. Elemental analysis calcd for $C_{10}H_{17}S_2ON_5Cu$: C, 34.22; H, 4.88; N, 19.96. Found: C, 34.17; H, 4.83; N, 20.01. Mass spectrum calcd for $CuL^2 + H^+$: 351.02. Found: 351.02.

CuL^3 (6). Complex **6** was prepared using the same method as described for **4** from H_2L^3 (0.435 g, 1.29 mmol) and copper(II) acetate monohydrate (0.285 g, 1.43 mmol) in methanol (25 mL). Complex **6** was isolated as a red-brown solid. Yield = 0.146 g (29%). IR cm^{-1}: 3324 and 1538 (NH), 2973 and 1428 (CH), 1382 and 1219 (CN), 1019 (CO), 974 (CS), 872 (CuS), 758 (CuN). UV−vis spectrum in acetonitrile (nm) (M^{-1} cm^{-1}): Shoulder around 263 (16,000), 309 (20,000), shoulder around 357 (13,000), 485 (5,500). EPR $g_{||}$ = 2.135 and $g_{\perp}$ = 2.032, g_{avg} = 2.066. Elemental analysis calcd for $C_{14}H_{17}S_2ON_5Cu$: C, 42.14; H, 4.29; N, 17.55. Found: C, 41.84; H, 4.22; N, 17.53. Mass spectrum calcd for $CuL^3 + H^+$: 399.02. Found: 399.02.

NiL^1 (7). Complex H_2L^1 (0.354 g, 1.29 mmol) was suspended in methanol (25 mL). To this suspension, nickel(II) acetate tetrahydrate (0.353 g, 1.42 mmol) was added with stirring, giving a dark brown precipitate. The suspension was refluxed for 4 h and then cooled to room temperature prior to being placed in a freezer overnight. The formed solid was filtered cold then washed with methanol. Yield = 0.326 g (77%). ^{1}H NMR (DMSO-d_6, 500 MHz): δ 1.21 (t, 3H) 2.00 (d, 6H), 2.81(d, 3H), 4.20 (q, 2H), 8.03 (s, 1H). IR cm^{-1}: 3414 and 1553 (NH), 2937 and 1402 (CH), 1382 and 1216 (CN), 1080 (CO), 1014 (CS), 872 (NiS), 782 (NiN). UV−vis spectrum in acetonitrile (nm) (M^{-1} cm^{-1}): 255 (38,000), shoulder around 326 (6,400), 389 (12,000). Elemental analysis calcd for $C_9H_{15}S_2ON_5Ni$: C, 32.55; H, 4.55; N, 21.09. Found: C, 32.09; H, 4.44; N, 20.54. Mass spectrum calcd for NiL^{1+} and $NiL^1 + H^+$: 331.01 and 332.02. Found: 331.01 and 332.01.

NiL^2 (8). Complex **8** was prepared using the method described for **7** from H_2L^2 (0.373 g, 1.29 mmol) and nickel(II) acetate tetrahydrate (0.353 g, 1.42 mmol) in methanol (25 mL). Complex **8** was isolated as a dark brown solid. Yield = 0.250 g (56%). ^{1}H NMR (DMSO-d_6, 500 MHz): δ 0.87 (t, 3H), 1.61 (m, 2H), 2.01 (br, 6H), 2.81 (s, 3H), 4.12 (q, 2H), 8.02 (s, 1H). IR cm^{-1}: 3341 and 1562 (NH), 29333 and 1493 (CH), 1307 and 1225 (CN), 1084 (CO), 1042 (CS), 855 (NiS), 735 (NiN). UV−vis spectrum in acetonitrile (nm) (M^{-1} cm^{-1}): 255 (32,000), shoulder around 330 (4,500), 388 (11,000). Elemental analysis calcd for $C_{10}H_{17}S_2ON_5Ni$: C, 34.70; H, 4.95; N, 20.24. Found: C, 34.49; H, 4.86; N, 19.92. Mass spectrum calcd for NiL^{2+} and $NiL^2 + H^+$: 345.02 and 346.03. Found: 345.01 and 346.03.

NiL^3 (9). Complex **9** was prepared using the method described for **7** from H_2L^3 (0.435 g, 1.29 mmol) and nickel(II) acetate tetrahydrate (0.353 g, 1.42 mmol) in methanol (25 mL). Complex **9** was isolated as a dark brown solid. Yield = 0.332 g (65%). ^{1}H NMR (DMSO-d_6, 500 MHz): δ 1.12 (t, 3H), 1.80 (s, 3H), 2.85 (s, 3H), 4.0 (q, 2H), 7.46 (br, 5H), 8.19 (q, 1H). IR cm^{-1}: 3408, 3256, and 1544 (NH), 2975 and 1500 (CH), 1332 and 1226 (CN), 1016 (CO), 975 (CS), 874 (NiS), 758 (NiN). UV−vis spectrum in acetonitrile (nm) (M^{-1} cm^{-1}): 252 (30,000), 342 (7,600), 405 (11,000). Elemental analysis calcd for $C_{14}H_{17}S_2ON_5Ni$: C, 42.66; H, 4.35; N, 17.77. Found: C, 42.85; H, 4.46; N, 17.57. Mass spectrum calc for NiL^{3+}: 393.02281. Found: 393.0214 and 394.0295.

ZnL^1 (10). Compound H_2L^1 (0.354 g, 1.29 mmol) was suspended in methanol (25 mL). To this suspension, zinc(II) acetate dihydrate (0.307 g, 1.40 mmol) was added with stirring, giving a yellow-orange precipitate. The suspension was refluxed for 4 h and then cooled to room temperature. The formed solid was filtered and then washed with methanol. Yield = 0.275 g (64%). ^{1}H NMR (DMSO-d_6, 500 MHz): δ 1.26 (t, 3H), 2.22 (s, 3H), 2.25/2.84 (s, 6H), 4.30 (q, 2H), 7.48 (br, 1H). IR cm^{-1}: 3337 and 1557 (NH), 2930 and 1494 (CH), 1397 and 1227 (CN), 1082 (CO), 1027 (CS), 841 (ZnS), 774 (ZnN). UV−vis spectrum in acetonitrile (nm) (M^{-1} cm^{-1}): 243 (12,000), 299 (9,900), 422 (8,700). Elemental analysis calcd for $C_9H_{15}S_2ON_5Zn$: C, 31.91; H, 4.46; N, 20.67. Found: C, 31.92; H, 4.45; N, 20.67. Mass spectrum calcd for $ZnL^1 + H^+$: 338.01. Found: 338.2153.

ZnL^2 (11). Complex **11** was prepared using the same method as described for **10** from H_2L^2 (0.373 g, 1.29 mmol) and zinc(II) acetate dihydrate (0.307 g, 1.40 mmol) in methanol (25 mL). Complex **11** was isolated as a yellow-orange precipitate. Yield = 0.424 g (91%). ^{1}H NMR (DMSO-d_6, 500 MHz): δ 0.92 (t, 3H), 1.66 (m, 2H), 2.20 (s, 3H), 2.22 (s, 6H), 2.85 (s, 3H), 4.21 (q, 2H), 7.49 (s, 1H). IR cm^{-1}: 3367, 3311, and 1549 (NH), 2973 and 1491 (CH), 1372 and 1209 (CN), 1122 (CO), 1079 (CS), 836 (ZnS), 783 (ZnN). UV−vis spectrum in acetonitrile (nm) (M^{-1} cm^{-1}): 243 (10,000), 299 (7,400), 423 (7,500). Elemental analysis calcd for $C_{10}H_{17}S_2ON_5Zn\cdot CH_3OH$: C, 34.33; H, 5.50; N, 18.20. Found: C, 33.99; H, 5.25; N, 18.12. Mass spectrum calcd for $ZnL^2 + H^+$: 352.02. Found: 352.07.

ZnL^3 (12). Complex **12** was prepared using the same method as described for **10** from H_2L^3 (0.435 g, 1.29 mmol) and zinc(II) acetate dihydrate (0.307 g, 1.40 mmol) in methanol (25 mL). Complex **12** was isolated as a yellow-orange precipitate. Yield = 0.322 g (62%). ^{1}H NMR (DMSO-d_6, 500 MHz): δ 1.14 (t, 3H), 2.03 (s, 3H), 2.87 (s, 3H), 4.08 (q, 2H), 7.45 (m, 5H), 7.62 (s, 1H). IR cm^{-1}: 3351 and 1541 (NH), 2971 and 1481 (CH), 1392 and 1221 (CN), 1019 (CO), 970 (CS), 801 (ZnS), 756 (ZnN). UV−vis spectrum in acetonitrile (nm) (M^{-1} cm^{-1}): 269 (11,000), 326 (8,100), 430 (7,300). Elemental analysis calcd for $C_{14}H_{17}S_2ON_5Zn$: C, 41.95; H, 4.27; N, 17.47. Found: C, 40.65; H, 4.08; N, 19.97. Mass spectrum calcd for $ZnL^3 + H^+$: 400.02. Found: 400.38.

Cu(GTSM). The synthesis and characterization of the complex **Cu(GTSM)** has previously been reported.[40] An alternate method was employed to prepare **Cu(GTSM)** in this study. The compound H_2GTSM (1.50 g, 6.46 mmol) was suspended in methanol (30 mL). To this suspension, copper(II) acetate monohydrate (1.29 g, 6.46 mmol) was added with stirring, giving a red-brown precipitate. The suspension was refluxed with stirring for 4 h and then cooled to room temperature. The solid was then filtered and washed with methanol. Yield = 1.90 g (91%). IR cm^{-1}: 3371, 1563 (NH), 2989, 1450 (CH), 1395, 1293 (CN), 1051 (CS), 833 (CuS), 736 (CuN). UV−vis spectrum in acetonitrile (nm) (M^{-1} cm^{-1}): 315 (16,500), shoulder around 369 (8000), 483 (7300) and shoulder around 530 (3200). EPR $g_{||}$ = 2.12 and $g_{\perp}$ = 2.036. Elemental analysis calcd for $C_6H_{10}N_6S_2Cu\cdot H_2O$: C, 23.11; H, 3.88; N, 26.95. Found: C, 23.51; H, 3.25; N, 25.55. Mass spectrum calcd for Cu(GTSM) + H^+: 293.97. Found: 294.25

Transmetalation. Stock solutions were prepared in acetonitrile for the Zn complex **10** (0.05 mM) and $Cu(OAc)_2\cdot 2H_2O$ (2.0 mM). A 2.00 mL aliquot of the Zn solution was titrated with 5 μL aliquots of the Cu solution at room temperature until the total concentration of the Zn and Cu complexes were equivalent. After each addition, the solution was agitated for 10−15 s and the UV−visible spectrum was recorded. During the titration, the color of the solution changed from yellow to red. A similar study was conducted using a 0.05 mM

https://dx.doi.org/10.1021/acs.inorgchem.0c00182
Inorg. Chem. XXXX, XXX, XXX−XXX

acetonitrile solution of the Ni complex **7**. Titration with the Cu solution resulted in no color change or change in the UV−visible spectrum even after the addition of 100 μL (2 equiv of Cu per Ni).

Physical Methods. Elemental analysis was performed by Midwest Micro lab (Indianapolis, IN). The electronic spectra were collected as acetonitrile solution in 1 cm quartz cuvettes using an Agilent 8453 diode array spectrometer. Mass spectrometry was performed by the Laboratory for Biological Mass Spectrometry at Texas A&M University (+ESI-MS) or using an Applied Biosystems Voyager System 6032 (MALDI-TOF). All EPR data were collected on powder samples at room temperature using a Bruker EMX X-band spectrometer. EPR spectra were simulated using EasySpin. The infrared spectra were recorded as powders on a Nicolet 360 FT-IR with a smart iTR attachment. NMR spectra were obtained on Varian 400 MHz spectrometer at 25 °C.

Electrochemical Measurements. Electrochemical data were collected using a Gamry Interface 1000E Potentiostat/Galvanostat/ZRA. Complexes were dissolved in acetonitrile (~2 mM) under air-free conditions in a standard three electrode cell with 0.1 M tetrabutylammonium hexafluorophosphate as the supporting electrolyte. Glassy carbon was used as the working electrode with a platinum wire counter electrode and a silver/silver chloride reference electrode. A small quantity of ferrocene was added as an internal standard, and all potentials are referenced versus ferrocenium/ferrocene (Fc^+/Fc^0).

Crystallographic Studies. A dark orange needle 0.31 × 0.05 × 0.05 mm^3 crystal of **4** grown from a solution of methylene chloride/methanol was mounted on a CryoLoop for collection of X-ray data on an Agilent Technologies/Oxford Diffraction Gemini CCD diffractometer. The CrysAlisPro[41] CCD software package (ver. 1.171.36.32) was used to acquire a total of 716 fifty-second frame ω-scan exposures of data at 100 K to a $2\theta_{max}$ = 56.32° using monochromated Mo Kα radiation (0.71073 Å) from a sealed tube. Frame data were processed using CrysAlisPro RED to determine final unit cell parameters: a = 8.2759(4) Å, b = 10.2427(3) Å, c = 16.8758(6) Å, α = 74.102(3)°, β = 89.740(4)°, γ = 85.364(3)°, V = 1371.07(9) $Å^3$, D_{calc} = 1.632 Mg/m^3, Z = 2 to produce raw *hkl* data that were then corrected for absorption (transmission min/max = 0.673/1.000; μ = 1.893 mm^{-1}) using SCALE3 ABSPACK.[42] The structure was solved by direct methods in the space group $P\bar{1}$ using SHELXS[43] and was refined by least-squares methods on F^2 using SHELXL.[43] Non-hydrogen atoms were refined with anisotropic atomic displacement parameters. All H's were located by difference maps and refined isotropically. For all 6,693 unique reflections (R(int) 0.030), the final anisotropic full matrix least-squares refinement on F^2 for 445 variables converged at $R1$ = 0.048 and wR2 = 0.082 with a GOF of 1.04.

Crystals of **6** suitable for X-ray analysis were grown from a methylene chloride/methanol solution and were mounted on a glass fiber for the collection of X-ray data on an Agilent Technologies/Oxford Diffraction Gemini CCD diffractometer. X-ray structural analysis for **6** was performed on a 0.31 × 0.17 × 0.03 mm^3 orange plate using a 941 thirty-second frame ω-scan data collection strategy at 100 K to a $2\theta_{max}$ = 58.42°. The complex crystallizes in the triclinic space group P1 with unit cell parameters: a = 10.2767(5) Å, b = 11.8398(5) Å, c = 14.8880(6) Å, α = 73.776(4)°, β = 78.850(4)°, γ = 75.204(4)°, V = 1667.09(13) $Å^3$, Z = 2, and D_{calc} = 1.571 Mg/m^3. Independent data (8,974) were corrected for absorption (transmission min/max = 0.792/1.000; μ = 1.571 mm^{-1}). The structure was solved by direct methods using SHELXS.[43] All non-hydrogen atoms were refined with anisotropic atomic displacement parameters. Imine NH hydrogen atoms were located by difference maps and refined isotropically. Methyl, methylene, and methine hydrogen atoms were placed in their geometrically generated positions and refined as a riding model, and these atoms were assigned U(H) = 1.5, 1.2, and 1.2 × Ueq of the carbon atom they are attached to, respectively. For reflections $I > 2\sigma(I)$ (R(int) 0.037), the final anisotropic full matrix least-squares refinement on F^2 for 429 variables converged at $R1$ = 0.035 and wR2 = 0.065 with a GOF of 1.04.

Crystals of **7** suitable for X-ray analysis were grown by slow evaporation of a methylene chloride/methanol solution. X-ray structural analysis for **7** was performed on a 0.38 × 0.05 × 0.01 mm^3 thin orange plate using an identical data acquisition strategy described above for **6** at 102 K to a $2\theta_{max}$ = 52.12°. The complex crystallizes in the space group $P2_1/c$ with unit cell parameters: a = 7.7351(2) Å, b = 20.8045(6) Å, c = 8.2308(3)Å, β = 93.119(3)°, V = 1322.58(7) $Å^3$, Z = 4 and D_{calc} = 1.668 Mg/m^3. Raw independent data (2,601) were corrected for absorption (transmission min/max = 0.939/1.000; μ = 1.502 mm^{-1}) using SCALE3 ABSPACK.[41] The structure was solved by Patterson methods using SHELXTL. All non-hydrogen atoms were refined with anisotropic atomic displacement parameters. Imine and methylene H's were located by difference maps and refined isotropically. Methyl hydrogen atoms were placed in their geometrically generated positions and refined as a riding model, and these atoms were assigned U(H) = 1.5 × Ueq For all 2,605 unique reflections (R(int) 0.032), the final anisotropic full matrix least-squares refinement on F^2 for 179 variables converged at $R1$ = 0.040 and wR2 = 0.085 with a GOF of 1.07.

A yellow prism 0.44 × 0.35 × 0.33 mm^3 crystal of **3** grown from a solution of methylene chloride/methanol was mounted on a glass fiber for collection of X-ray data on an Agilent Technologies/Oxford Diffraction Gemini CCD diffractometer. A total of 824 thirty-second frame ω-scan exposures of data at 102 K to a $2\theta_{max}$ = 61.10° using monochromated Mo Kα radiation (0.71073 Å) from a sealed tube. The final unit cell parameters were: a = 9.91024(14)Å, b = 16.6144(2) Å, c = 20.7808(3) Å, β = 96.2668(13)°, V = 3401.16(8) $Å^3$, D_{calc} = 1.318 Mg/m^3, Z = 8 to produce raw *hkl* data that were then corrected for absorption (transmission min/max = 0.970/1.000; μ = 0.322 mm^{-1}) using SCALE3 ABSPACK.[41] The structure was solved by direct methods in the space group $P2_1/c$ using SHELXS[34] and was refined by least-squares methods on F^2 using SHELXL.[34] Non-hydrogen atoms were refined with anisotropic atomic displacement parameters. All hydrogen atoms (except for methyl H's) were located by difference maps and refined isotropically. For all 10,411 unique reflections (R(int) 0.042), the final anisotropic full matrix least-squares refinement on F^2 for 483 variables converged at $R1$ = 0.050 and wR2 = 0.088 with a GOF of 1.04.[7]

Cell Studies. A549 and IMR-90 cells were purchased from the American Type Culture Collection (ATCC, Manassas, VA). Cells were grown in the appropriate medium supplemented with 10% fetal bovine serum (FBS, Life Technologies, Grand Island, NY), 62.5 μg/mL penicillin, and 100 μg/mL streptomycin (Life Technologies) in a humidified incubator at 37 °C with 5% CO_2. The growth media were as follows: Dulbecco's modified Eagle's medium (DMEM, Life Technologies) for A549 cells, and Eagle's minimal essential medium (EMEM) with Eagle's balanced salt solution (EBSS), 2 mM L-glutamine, 1500 mg/L sodium bicarbonate (Lonza, Walkersville, MD), supplemented with 1 mM sodium pyruvate (Life Technologies), and nonessential amino acids (Life Technologies) for IMR-90 cells. For treatment, metal complexes were dissolved first in 100% DMSO and then diluted in aqueous medium. The final concentration of DMSO used in the assays was always less than 0.5% v/v.

Antiproliferative activity of the metal complexes was evaluated using a previously published 3-(4,5-dimethylthiazol-2-yl)-2,5-diphenyltetrazolium bromide (MTT) assay protocol.[44,45] Cells were seeded in quadruplicate wells in 96-well plates and allowed to adhere overnight. To account for intrinsic differences in growth rates, cells were plated at the following densities to achieve comparable MTT absorbance values (OD570 between 0.5 and 1) for untreated cells: A549, 1000 cells/well; IMR-90, 5000 cells/well. After 72 h of treatment with the various complexes or vehicle control, MTT (Sigma/Millipore Sigma, St. Louis, MO) was added for 4 h prior to cell lysis. All readings were normalized to the vehicle treatment. Dose response curves represent the results of at least three independent experiments.

Assessment of the relative number of live cells was determined by cell counting and assessing trypan blue exclusion (the dye is absorbed by dead or dying cells but excluded from live cells). A549 cells were seeded at a density of 3000 cells/well in 24-well plates and allowed to adhere overnight. After 72 h of treatment with complexes, cell count and viability were determined in duplicate samples for each treatment

https://dx.doi.org/10.1021/acs.inorgchem.0c00182
Inorg. Chem. XXXX, XXX, XXX−XXX

Table 1. Selected Bond Distances and Angles for H_2L^3, 4, 6, and 7

bond distance	H_2L^3	4	6	7
M−N1	N/A	1.967(2)	1.9755(14)	1.868(3)
M−N3	N/A	1.959(2)	1.9590(13)	1.859(2)
M−S1	N/A	2.2529(7)	2.2725(4)	2.1554(8)
M−S2	N/A	2.2795(7)	2.2871(5)	2.1740(8)
S1−C5 (C10)[a]	1.6736(13)	1.761(3)	1.7584(17)	1.760(3)
S2−C6 (C11)[a]	1.6568(14)	1.758(3)	1.7376(16)	1.753(3)
O1−C6 (C11)[a]	1.3160(13)	1.332(3)	1.3339(19)	1.334(4)
N1−C1	1.2898(17)	1.293(3)	1.298(2)	1.303(4)
N1−N2	1.3660(15)	1.362(3)	1.3611(19)	1.376(4)
N2−C5 (C10)[a]	1.3672(17)	1.318(3)	1.319(2)	1.319(4)
N5−C5 (C10)[a]	1.3251(18)	1.338(3)	1.331(2)	1.338(4)
C1−C2	1.4778(18)	1.477(3)	1.472(2)	1.473(4)
C1−C3	1.496(2)	1.492(4)	1.492(2)	1.488(4)
Bond Angles				
N3−M−N1	N/A	80.31(9)	79.68(6)	83.38(11)
N1−M−S1	N/A	84.58(6)	83.31(4)	87.18(8)
N3−M−S2	N/A	84.59(6)	84.49(4)	87.27(8)
S1−M−S2	N/A	108.85(3)	111.359(16)	102.15(3)

[a]Numbers are different due to presence of benzene rings in H_2L^3 and 6.

using 0.4% trypan blue solution (Life Technologies) and the TC10 Automated Cell Counter (BioRad, Hercules, CA).

The clonogenic assay determines the ability of single cells to form colonies and was used to measure cell survival. A549 cells were plated at low density (300 cells/well) in 6-well tissue culture plates and allowed to adhere overnight. Metal complexes or vehicle control were added to the cell culture medium. After 10 days of treatment, cells were fixed with 4% paraformaldehyde in PBS and stained with 0.04% Accustain Crystal Violet Solution (Sigma-Aldrich), washed with deionized water, and air-dried. Colonies were quantified using the ColonyArea plugin[46] for ImageJ software (National Institutes of Health, Bethesda, MD).

RESULTS AND DISCUSSION

A series of hybrid thiosemicarbazone-alkylthiocarbamate ligands (H_2L^1−H_2L^3) with variation in the alkoxy chain length of ethyl (H_2L^1) and propyl (H_2L^2) as well as incorporation of a phenyl group in the backbone (H_2L^3) was prepared in high yields using readily available, inexpensive organic reagents. Briefly, a mono-keto-thiosemicarbazide[32] is condensed with a hydrazinecarbothioic acid *O*-alkyl ester[39] to yield the hybrid ligand. The ligand is then refluxed in methanol with the corresponding metal acetate salt to yield Cu(II) (**4**−**6**), Ni(II) (**7**−**9**), and Zn(II) (**10**−**12**) metal complexes.

The ^{1}H NMR of H_2L^1 in DMSO-d_6 (Figure S1) displays a combination of prototypical chemical shifts associated with BTSCs and alkylthiocarbamate ligands.[38] The backbone methyl groups remain in similar magnetic environments and are observed as a single peak at 2.17 ppm. The methyl protons from the pendent amine are observed as a doublet at 3.00 ppm, while the methyl protons from the alkoxide moiety yield a triplet upfield at 1.28 ppm. The methylene protons from the alkoxide moiety appear as a quartet at 4.5 ppm. The pendent amine proton is observed at 8.35 ppm, the imino proton of the thiosemicarbazide side of the ligand appears as a singlet 10.21 ppm, while the imino proton of the alkoxide side displays as two singlets at 11.31 and 11.62 ppm due to tautomerization.[38] The ^{13}C NMR of H_2L^1 (Figure S2) exhibits a chemical shift for the alkoxy carbon at 66.2 and 67.3 ppm due to the tautomerization. The alkyl peaks of the backbone carbons, —$NHCH_3$, and CH_3 from the ethyl alkoxide are observed as a series of peaks from 11.8−31.7 ppm. The C═N resonance displays three signals at 189.0, 186.9, and 178.8 ppm with three signals for the C═S carbon at 153.8, 152.2, and 148.1 ppm due to tautomerization. The ^{1}H and ^{13}C NMR of H_2L^2 and H_2L^3 are similar to those of H_2L^1 and consistent with their proposed structures (Figures S3−S6).

The ^{1}H NMR of complex **10** (Figure S10) is consistent with deprotonation of the imino hydrogens of H_2L^1 upon coordination to Zn(II) as the peaks at 10.21 and 11.31/11.62 ppm are not observed. The same trend is observed in the ^{1}H NMR of the zinc complexes **11** and **12** (Figures S12 and S14). The nickel derivatives **7**−**9** display similar ^{1}H NMR spectra as their zinc counterparts, with the notable addition of a peak at 8.55 ppm (Figures S9−S11) attributed to a small amount of residual acetic acid.

The FT-IR of H_2L^{1-3} (Figure S15−S17) displays two N−H stretches (3382 and 3253 cm^{-1} for H_2L^1) characteristic of BTSCs and a C−O stretch (1130 cm^{-1} for H_2L^1) representative of the alkylthiocarbamate moiety. Upon metalation of H_2L^1 with copper (**4**) (Figure S18), the N−H stretch at 3382 cm^{-1} is absent consistent with deprotonation of the imino hydrogen. However, the N−H stretch is observed at 3305 cm^{-1} associated with the pendent amine remains. The C−O stretch remains largely unaffected at 1132 cm^{-1}. Further, the addition of stretches at 846 and 782 cm^{-1} are attributed to Cu−S and Cu−N bonds, respectively. Similar stretches, such as the appearance of Ni−S/Ni−N and Zn−S/Zn−N are observed in the remaining FT-IR spectra and can be found in the Supporting Information (Figures S18−S26).

The electronic spectra of metal complexes **4**−**12** were collected in acetonitrile. Each display two ligand-to-ligand charge transfer bands and one metal-to-ligand charge transfer band. The electronic spectra of the Cu complexes (**4**−**6**) are displayed in Figure S29. Complex **4** displays two ligand-to-ligand charge transfer bands in the UV region at 248 and 309 nm. The lower energy band has a shoulder at 346 nm. An asymmetric ligand-to-metal charge transfer band is observed at 473 nm. The spectrum of **5** is similar to that of **4**. The backbone phenyl substituent of **6** results in additional features in the UV region. Additionally, the metal-to-ligand band is red-

https://dx.doi.org/10.1021/acs.inorgchem.0c00182
Inorg. Chem. XXXX, XXX, XXX−XXX

shifted to 485 nm. The electronic spectra of the Ni complexes **7**−**9** (Figure S30) and Zn complexes **10**−**12** (Figures S31) are qualitatively similar to the Cu counterparts, although the metal-to-ligands bands are blue-shifted to 388−404 nm and 422−430 nm, respectively.

The EPR spectra of the copper derivatives **4**−**6** recorded on powder samples at room temperature are consistent with a square planar geometry with an unpaired electron in the $d_{x^2-y^2}$ orbital. The spectrum of **5** (Figure S34A) was simulated with $g_{\|} = 2.116$ and $g_{\perp} = 2.030$ ($g_{avg} = 2.059$). The spectrum of **6** (Figure S34B) is similar to $g_{\|} = 2.135$ and $g_{\perp} = 2.032$ ($g_{avg} = 2.066$). The spectrum of **4** (Figure S33) was simulated as an axial signal with $g_{\|} = 2.091$ and $g_{\perp} = 2.061$ ($g_{avg} = 2.071$), which is near the g average (where $g_{avg} = 1/3[g_{\|} + 2g_{\perp}]$) value of the other two complexes. Overall, the data indicates a similar electronic environment to Cu(ATSM), g average = 2.056,[47] and our previously reported bis(alkylthiocarbamate) copper complexes, g average = 2.061.[38]

Crystallography. The solid state structures of $\mathbf{H_2L^3}$, **4**, **6**, and **7** were determined by single crystal X-ray diffraction. The copper complexes **4** and **6** crystallized as a dark orange needle and an orange plate, respectively, in the space group $P\bar{1}$. The nickel complex **7** crystallized as an orange plate in the space group $P2_1/c$. The ligand, $\mathbf{H_2L^3}$ crystallized as a yellow prism in the space group $P2_1/c$. All four complexes crystallize without inclusion of solvent molecules. Crystallographic data and structural refinement details are provided in the Supporting Information (Table S1). Selected bond distances and angles are listed in Table 1 along with a more comprehensive list in Tables S2−S5. Figure 1 shows ORTEP representations of **4** and **7**, the copper and nickel complexes of $\mathbf{H_2L^1}$. ORTEP representations of $\mathbf{H_2L^3}$ and **6** are provided in Figures S36−S38.[48]

The Cu and Ni complexes **4** and **7** share a common square planar environment in an N_2S_2 chelate. The Cu−N and Cu−S bonds distances are 0.10(1) Å longer than those of the corresponding Ni−N and Ni−S bond distances consistent with the difference in ionic radii of Cu(II), 71 pm, and Ni(II), 63 pm, in square planar environments. The Cu−N and Cu−S bond distances in **6** are statistically equivalent to those of **4**, which are also similar to those of Cu(ATSM)[49] and bis(alkylthiocarbamate) Cu complexes.[38] Likewise, the metal−ligand bond distances of **7** match those of Ni-(ATSM).[50] Within the ligand framework, all bond distances across the series regardless of the chelated metal are statistically equivalent and consistent with a conjugated π-system of alternating single and double bonds.

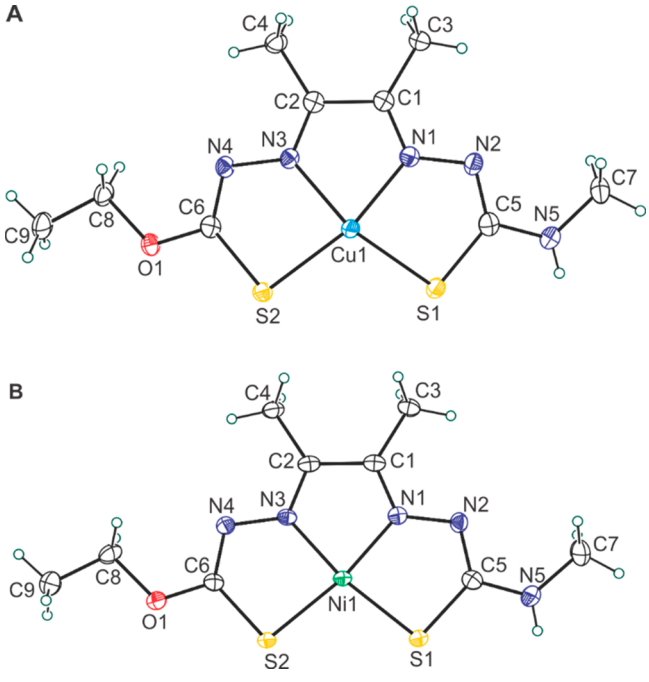

Figure 1. ORTEP[48] representations of **4** (A) and **7** (B).

The structure of all three metal complexes is rigorously planar. The sum of the four Cu-ligand bond angles in **4** is 358.33(0.12)°. For **4**, the best fit plane, calculated using Platon,[51] for all 18 non-hydrogen atoms has a standard deviation of ±0.067 Å with the largest deviation of ±0.116 Å for C9. For complex **7**, the best fit plane of all 18 non-hydrogen atoms has a standard deviation of ±0.128 Å with the largest deviation being ±0.326 Å for C9. Excluding the phenyl ring in **6** (C4−C9), the best fit plane for the remaining 18 non-hydrogen atoms has a standard deviation of ±0.137 Å with the largest deviation of ±0.329 Å for C12 (C7).

Electrochemistry. The relationship between electrochemical properties of the BTSC complexes and the biological activity of their metal complexes has been well documented.[2−5,7,10,12,17−20,24,32,52−54] The cyclic voltammograms (CVs) of copper complexes **4** and **6** and nickel complexes **7** and **9** can be found in Figure 2, and the CVs of all these complexes were recorded in anhydrous acetonitrile at a scan rate of 200 mV s^{-1}. Glassy carbon was used as the working electrode, with a platinum wire counter electrode and a silver/silver chloride reference electrode. The CVs of the corresponding zinc complexes are reported in the Supporting Information (Figure S40). The CVs of the free ligands were not recorded but are expected to be similar to that of the Zn complex as for H_2ATSM and Zn(ATSM).[55] The Cu complexes display a single quasi-reversible reduction, where the Ni derivatives display two quasi-reversible reduction events in the solvent window. In contrast, the Zn complexes display two irreversible reductions attributed to ligand-centered events. A periodic trend is observed with Cu having the most anodic events, followed by Ni, and then Zn. As shown in Table 2, the $Cu^{II/I}$ couple is 0.57−0.63 V more anodic than that of the first redox event of the corresponding Ni complexes. The first reduction event for the Ni complexes is proposed to be ligand centered[41] with a metal-centered $Ni^{II/I}$ couple 1.28−1.36 V that is more cathodic than those of the corresponding $Cu^{II/I}$ couples. The ligand-centered reduction of the Ni complexes is 0.41−0.42 V more anodic than that of the first Zn reduction.

Across the ligand series, there is a clear effect of electron donor ability from the R groups on reduction potential. The alkyl extension of R_2 from ethyl to propyl resulted in a minimal or no effect on reduction potential.[38] This is exemplified in the 0.01 V shifts for Cu complexes **4** and **5** (data not shown). All other redox couples were unchanged by alkyl extension. The incorporation of a phenyl group in R_1 caused a significant anodic shift in reduction potential for all complexes. The smallest anodic shift observed with the installment of the phenyl group is for Cu complexes where the $Cu^{II/I}$ couple of **6** is shifted by 0.08 V when compared to **4**. The remaining chelates display anodic shifts of close to 0.1 V or higher when comparing the ligand framework of $\mathbf{H_2L^3}$ to $\mathbf{H_2L^1}$.

https://dx.doi.org/10.1021/acs.inorgchem.0c00182
Inorg. Chem. XXXX, XXX, XXX−XXX

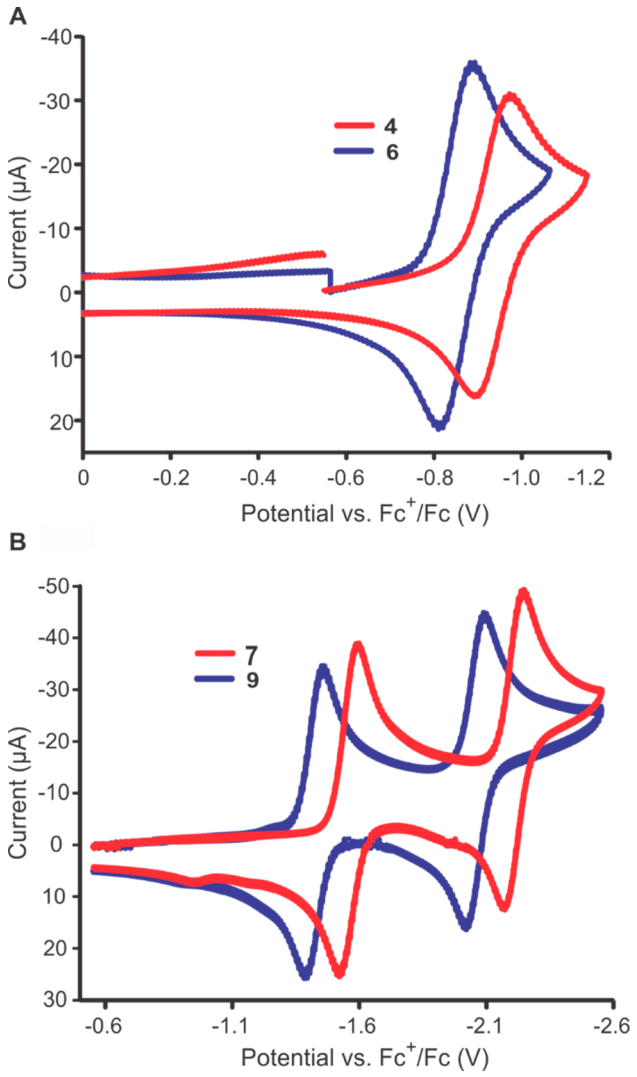

Figure 2. Cyclic voltammograms recorded in anhydrous acetonitrile at a scan rate of 200 mV s^{-1} displaying the anodic shift caused by installment inclusion of the phenyl group in the ligand framework of both the copper (A) and nickel chelates (B).

Table 2. Reduction Potentials for 4−12 vs Fc^+/Fc^0

ligand	$Cu^{II/I}$ [a]	NiL/NiL^- [a]	$Ni^{II/I}$ [a]	ZnL/ZnL^- [b]	ZnL^-/ZnL^{2-} [b]
H_2L^1	−0.930	−1.56	−2.21	−1.98	−2.37
H_2L^2	−0.940	−1.56	−2.22	−1.98	−2.40
H_2L^3	−0.850	−1.42	−2.12	−1.83	−2.22

[a] = $E_{1/2}$ [b] = E_{pc}

In comparison with the previously reported analogous BTSC and bis(alkylthiocarbamate) complexes, reduction potentials of complexes with the hybrid thiosemicarbazone−alkylthiocarbamate ligands lay between the parent complexes. For example, the $Cu^{II/I}$ reduction potential of **4**, −0.930 V, sits between those of the BTSC complex Cu(ATSM), −1.11 V,[12] and the bis(alkylthiocarbamate) derivative CuETCB, −0.880 V.[38] Despite the inclusion of the alkylthiocarbamate moiety, the hybrid ligand system allows tuning of the $Cu^{II/I}$ reduction potentials to values similar to that of Cu(GTSM), −0.950 V, while introducing a new functional group that may significantly alter anticancer properties. Notably, the solubility of our hybrid complexes is similar to other BTSC complexes and greater than the bis(alkylthiocarbamate) Cu complex, Cu(ETCB) in DMSO. Whereas, the aqueous solubility is greatest for Cu(GTSM), followed by our hybrid complexes and the bis(alkylthiocarbamate) Cu complex, Cu(ETCB), being the least soluble in water (see the Supporting Information).

Cell line Evaluation. To investigate potential antiproliferative effects of **4**−**12**, each complex was screened in a lung adenocarcinoma cell line (A549) and in a nonmalignant lung fibroblast cell line (IMR-90). A representative MTT assay (Figure 3) displays the activity of the complexes **4**, **7**, and **10**, while other data can be found in Table 3 and in the Supporting Information (Figures S41 and S42). The general trend observed across the hybrid ligand series is that the copper complexes are most active, followed by zinc, with the nickel derivatives being the least active. However, zinc complex **12** surprisingly had similar activity to the corresponding copper complex **6**. The Cu complexes **4**−**6** have respective GI_{50} values of 0.082, 0.29, and 0.065 μM for A549, compared to >2.0, > 2.0, and 1.3 μM of the IMR-90 cell line, Table 3. Further, compared to Cu(ATSM) or the commonly used chemotherapy drug, cisplatin, the copper chelates **4**−**6** are both more potent and more selective for cancer cells (Figure S43, Table 3.) Compared to Cu(GTSM), copper chelates **4**−**6** are slightly less potent but markedly more cancer-selective (Figure S44, Table 3). The nickel derivatives **7**−**9** display greater GI_{50} values for both A549 and IMR90 cell lines, with no clear trend in selectivity. The difference in performance for the Cu and Ni complexes is attributed to the relatively accessible reduction potential of the Cu complexes as compared to Ni (Table 2). It has previously been suggested for ATSM derivatives of Cu that activity is dependent on reduction potential.[19,27,28] The Zn complexes **10**−**12** showed improved potency compared to that of the corresponding Ni complexes and, depending on the ligand, had either reduced or similar potency/selectivity compared to that of the corresponding Cu complexes (Table 3).

To further confirm the biological activity results, additional assays in A549 lung cancer were performed. Trypan blue exclusion was used to determine the number of viable cells remaining following treatment with the H_2L^1 series of metal complexes. As expected, the copper complex (**4**) was most active and the zinc complex (**10**) was also active, whereas the Ni complex (**7**) had no consistent effect (Figure 3C). Cell survival in a clonogenic (colony formation) assay was also measured and demonstrated the same result that the copper complex (**4**) was most active, followed by the zinc complex (**10**), and the Ni complex (**7**) had no activity even when used at much higher concentrations (Figure 3D,E).

To investigate whether the activity of the Zn complexes might be explained by transmetalation with Cu (which is present in the cell culture media), we performed additional studies. Previously, it has been shown that Cu(II) can displace Zn(II) from Zn(BTSC).[56−58] For our hybrid species, the titration of the Zn complex **10** with Cu(II)acetate in acetonitrile results in a change in the UV−vis absorption spectrum consistent with transmetalation reaction at equimolar concentrations of Cu (Figure 4). Notably, the titration of Ni complex **7** with Cu(II)acetate does not show any transmetalation (Figure S45). Our hypothesis is that the Zn complexes, **10**−**12**, are transmetalated to varying degrees and that the Cu complex is the active species. In this way, complexes **10** − **12** behave similarly to bis-(thiosemicarbazonato) Zn complexes in terms of trans-

https://dx.doi.org/10.1021/acs.inorgchem.0c00182
Inorg. Chem. XXXX, XXX, XXX−XXX

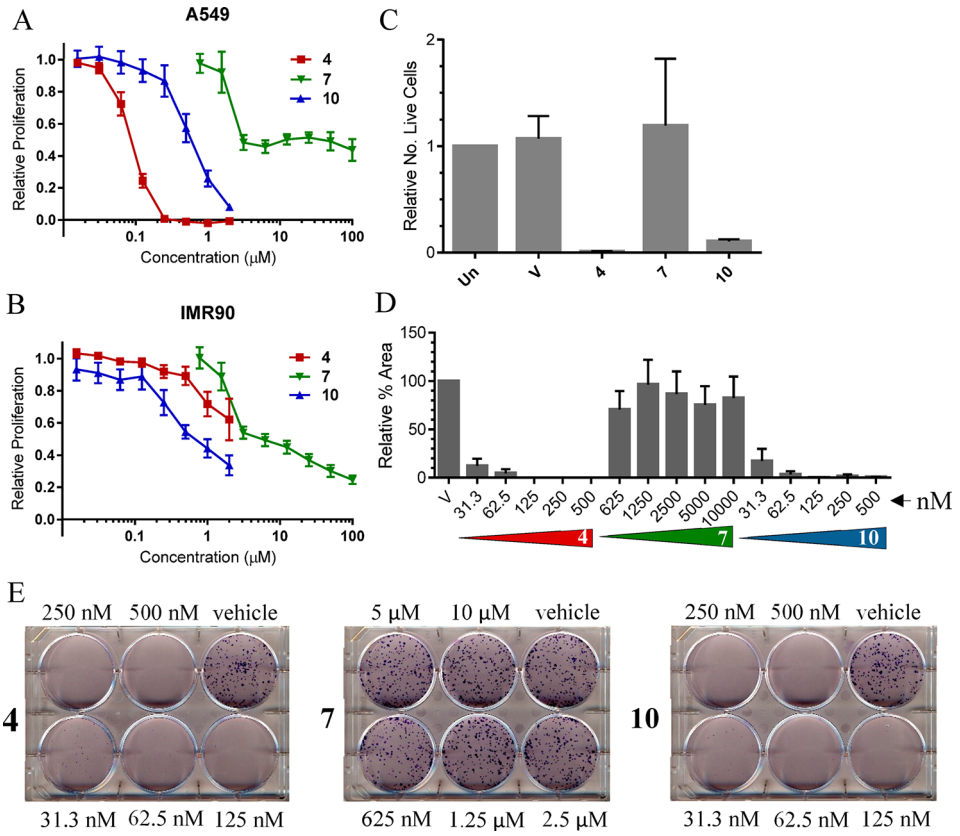

Figure 3. Results from cell studies. Cell proliferation results of lung adenocarcinoma cell line A549 (A) and nonmalignant lung fibroblast cell line IMR90 (B) treated with Cu complex **4** (red trace), Ni complex **7** (green trace), and Zn complex **10** (blue trace). Trypan blue exclusion results in A549 cells (C) either untreated (Un), treated with vehicle (V), or complexes **4** (1 μM), **7** (5 μM), and **10** (1 μM). Complex **7** was used at a higher concentration due to its low activity. Clonogenic assay result summary in A549 cells (D) and representative clonogenic assay plates (E) treated with increasing concentrations of complexes **4**, **7**, and **10**. Experiments were performed as described in the Materials and Methods section. Error bars represent the standard error of the mean.

Table 3. GI_{50} Values (μM) for 4−12[a]

complex	metal (M)	A549	IMR90	ratio of IMR90/A549
ML^1	Cu (**4**)	0.082	>2.0	>24
	Ni (**7**)	3.0	5.3	1.7
	Zn (**10**)	0.59	0.68	1.2
ML^2	Cu (**5**)	0.29	>2.0	>6.9
	Ni (**8**)	10.1	13	1.3
	Zn (**11**)	0.45	0.52	1.2
ML^3	Cu (**6**)	0.065	1.3	20
	Ni (**9**)	37	>100	>2.7
	Zn (**12**)	0.055	1.1	20
ATSM	Cu	0.48	2.0	4.2
	Ni	50	21	0.42
	Zn	7.6	6.2	0.82
GTSM	Cu	0.02	0.015	0.75
ETCB	Cu	0.17	1.0	5.9
Cisplatin	Pt	10.9	13.9	1.3

[a]Values were determined from the curves shown in Figure 3 and Supporting Information Figures S41−S44.

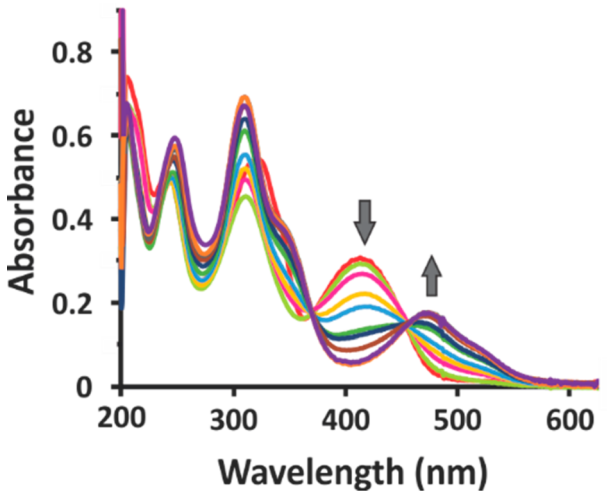

Figure 4. Experimental UV−vis absorption spectra of 2 mL of 0.05 mM **10** in acetonitrile upon titration with 11, 5 μL aliquots of 2.0 mM $Cu(OAc)_2{\cdot}2H_2O$ in acetonitrile to give **4**.

metalation with Cu (II).[56−58] The Ni complexes, **7**−**9**, cannot be easily transmetalated by Cu and so have low activity. If our hypothesis is correct, we predicted that the free ligands would be able coordinate copper from the culture medium and would have biological activities similar to the Zn complexes. As predicted, H_2L^1, H_2L^2, and H_2L^3 had similar effects as the corresponding Zn complexes in MTT assays (Figure S46).

Finally, our two most active copper complexes, **4** and **6**, were submitted to the National Cancer Institute's Developmental Therapeutics Program to evaluate selectivity for certain cancer types using the NCI60 human tumor cell line panel.[59] Both complexes demonstrated potent growth inhibitory and cytotoxic effects against the majority of cell lines in the panel

https://dx.doi.org/10.1021/acs.inorgchem.0c00182
Inorg. Chem. XXXX, XXX, XXX−XXX

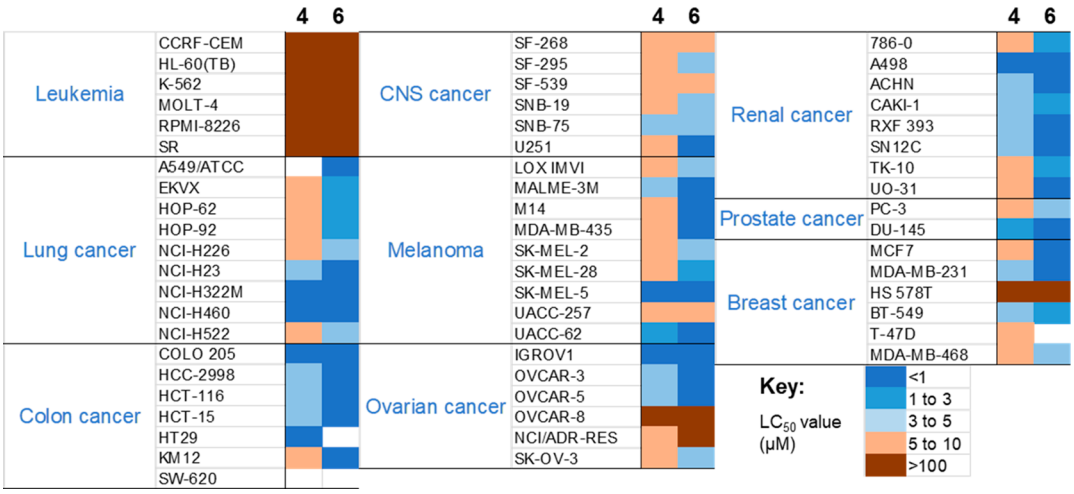

Figure 5. Results from NCI60 human cell line screen. Compounds **4** and **6** were submitted to NCI, and screen was performed as described.[59]

(Figure 5 and Table S7). For **4**, the average GI_{50} (50% growth inhibition compared to untreated control cells), TGI (total growth inhibition), and LC_{50} (50% reduction in cell number compared to starting cells) concentrations across all cell lines in the panel were 479 nM, 1.70 μM, and 5.81 μM, respectively. For **6**, these values were 229 nM (GI_{50}), 631 nM (TGI), and 2.75 μM (LC_{50}). The biggest difference in cell line sensitivities was apparent for LC_{50} values, with leukemia cell lines being far less sensitive to the cytotoxic effects compared to most solid tumor types (Figure 5). A somewhat similar pattern has been reported for other copper complexes that have been screened the NCI60 panel,[60−62] but the reasons for the relative resistance of leukemic cells vs solid tumor lines are unclear. Regarding **4** and **6**, the similarity of their NCI60 profiles suggest a shared mechanism of action and the dose responses indicate that **6** is more potent than **4**.

CONCLUSIONS

A new hybrid thiosemicarbazone−alkylthiocarbamate ligand system has been successfully synthesized, and corresponding Cu, Ni, and Zn complexes have been prepared. The reduction potential of the metal center in the hybrid ligands is intermediate between the corresponding BTSC and alkylthiocarbamate derivatives. This allows for tuning of reduction potential combined with the introduction of various structural features that may be important for selective bioactivity. The obtained single crystals displayed statistically indistinguishable bond distances and angles to those of the previously reported homologues that have been employed in biological applications. The evaluation of the copper, nickel, and zinc complexes for antiproliferative activity revealed the copper derivatives to be not only potent, but also selective for the malignant cells compared to nonmalignant cells. The selectivity of the Cu complexes may be due to the tuning of the reduction potential; although, this needs to be further verified. In general, antiproliferative activity will depend on physical and chemical properties that determine solubility, cell uptake, and potential for metals to be released intracellularly. The mechanism for selectivity for cancer cells compared to noncancer cells is uncertain but may be due to differences in intracellular redox environment, glutathione content, and/or ability to tolerate stress.[14,33,34,37,63] The zinc derivatives we tested also had some biological activity, though typically less than the copper complexes, and results suggest the zinc complex activity is due to transmetalation by copper from the cell culture medium. The similarity in the activity and selectivity of CuL^3 and ZnL^3 suggests transmetalation may be occurring at greater extent with this ligand. The nickel derivatives were far less biologically active than the corresponding zinc or copper complexes, likely because they were not amenable to transmetalation by copper. In summary, this new ligand system will facilitate the synthesis of new molecular libraries and shows promise for the development of new anticancer agents.

ASSOCIATED CONTENT

Supporting Information

The Supporting Information is available free of charge at https://pubs.acs.org/doi/10.1021/acs.inorgchem.0c00182.

Figures of NMR spectra, FT-IR spectra, electronic spectra, EPR data, ORTEP[1] representation, cyclic voltammograms, MTT assay results, experimental UV−vis absorption spectra, and results from the NCI60 human line screen, tables of crystal data and structural refinement, selected bond distances and bond angles, GI_{50} values, and alternative method for calculating GI_{50} values, and discussions of solubility studies (PDF)

Accession Codes

CCDC 1912249−1912252 contain the supplementary crystallographic data for this paper. These data can be obtained free of charge via www.ccdc.cam.ac.uk/data_request/cif, or by emailing data_request@ccdc.cam.ac.uk, or by contacting The Cambridge Crystallographic Data Centre, 12 Union Road, Cambridge CB2 1EZ, UK; fax: +44 1223 336033.

AUTHOR INFORMATION

Corresponding Authors

Robert M. Buchanan − *Department of Chemistry, University of Louisville, Louisville, Kentucky 40292, United States;* orcid.org/0000-0001-8653-5388; Email: robert.buchanan@louisville.edu

Paula J. Bates − *Department of Medicine and James Graham Brown Cancer Center, University of Louisville, Louisville, Kentucky 40202, United States;* Email: paula.bates@louisville.edu

https://dx.doi.org/10.1021/acs.inorgchem.0c00182
Inorg. Chem. XXXX, XXX, XXX−XXX

Craig A. Grapperhaus − *Department of Chemistry, University of Louisville, Louisville, Kentucky 40292, United States;* orcid.org/0000-0003-4889-2645; Email: craig.grapperhaus@louisville.edu

Authors

Sarah A. Andres − *Department of Medicine and James Graham Brown Cancer Center, University of Louisville, Louisville, Kentucky 40202, United States*

Kritika Bajaj − *Department of Chemistry, University of Louisville, Louisville, Kentucky 40292, United States;* orcid.org/0000-0001-8073-9320

Nicholas S. Vishnosky − *Department of Chemistry, University of Louisville, Louisville, Kentucky 40292, United States*

Megan A. Peterson − *Department of Medicine and James Graham Brown Cancer Center, University of Louisville, Louisville, Kentucky 40202, United States*

Mark S. Mashuta − *Department of Chemistry, University of Louisville, Louisville, Kentucky 40292, United States;* orcid.org/0000-0002-2724-7252

Complete contact information is available at: https://pubs.acs.org/10.1021/acs.inorgchem.0c00182

Author Contributions

S.A.A. performed all biological assays and contributed to writing the manuscript. K.B. and N.S.V. performed all other experiments and contributed to writing the manuscript. M.A.P. assisted with biological assays. M.S.M. performed all crystallographic studies. R.M.B., P.J.B., and C.A.G. conceived the project, supervised experimental studies, and contributed to writing the manuscript. All authors have approved the final version of the manuscript.

Author Contributions

[§]S.A.A., K.B., and N.S.V. contributed equally.

Funding

This research was supported in part by the National Science Foundation (CHE-1665136 (C.A.G.) and CHE-1800245 (R.M.B.)), the National Cancer Institute (R25-CA134283 (P.J.B.), and the National Institutes of Health U01 HL127518 (P.J.B), which was funded by NIMHD, NHGRI, NHLBI, NIA, NIAAA, NIBIB, NICHD, NIDA, NINDS, NINR, and NLN. The Department of Energy (DEFG02-08CH11538) and the Kentucky Research Challenge Trust Fund are acknowledged for upgrade of X-ray facilities (M.S.M.).

Notes

The authors declare the following competing financial interest(s): Results described in this manuscript are included in a pending US patent application (20200062703) entitled "Compounds, Compositions, Methods for Treating Diseases, and Methods for Preparing Compounds."

REFERENCES

(1) *Cancer Facts & Figures 2019*; American Cancer Society: Atlanta, 2019.

(2) Bonnitcha, P. D.; Vavere, A. L.; Lewis, J. S.; Dilworth, J. R. In vitro and in vivo evaluation of bifunctional bisthiosemicarbazone Cu-64-complexes for the positron emission tomography imaging of hypoxia. *J. Med. Chem.* **2008**, *51*, 2985−2991.

(3) Fujibayashi, Y.; Taniuchi, H.; Yonekura, Y.; Ohtani, H.; Konishi, J.; Yokoyama, A. Copper-62-ATSM: A new hypoxia imaging agent with high membrane permeability and low redox potential. *J. Nucl. Med.* **1997**, *7*, 1155−1160.

(4) Handley, M. G.; Medina, R. A.; Mariotti, E.; Kenny, G. D.; Shaw, K. P.; Yan, R.; Eykyn, T. R.; Blower, P. J.; Southworth, R. Cardiac Hypoxia Imaging: Second-Generation Analogues of Cu-64-ATSM. *J. Nucl. Med.* **2014**, *55*, 488−494.

(5) Ikawa, M.; Okazawa, H.; Kudo, T.; Kuriyama, M.; Fujibayashi, Y.; Yoneda, M. Evaluation of striatal oxidative stress in patients with Parkinson's disease using [Cu-62]ATSM PET. *Nucl. Med. Biol.* **2011**, *38*, 945−951.

(6) McInnes, L. E.; Noor, A.; Kysenius, K.; Cullinane, C.; Roselt, P.; McLean, C. A.; Chiu, F. C. K.; Powell, A. K.; Crouch, P. J.; White, J. M.; Donnelly, P. S. Potential Diagnostic Imaging of Alzheimer's Disease with Copper-64 Complexes That Bind to Amyloid-beta Plaques. *Inorg. Chem.* **2019**, *58*, 3382−3395.

(7) Paterson, B. M.; Cullinane, C.; Crouch, P. J.; White, A. R.; Barnham, K. J.; Rose, P. D.; Noonan, W.; Binns, D.; Hicks, R. J.; Donnelly, P. S. Modification of Biodistribution and Brain Uptake of Copper Bis(thiosemicarbazonato) Complexes by the Incorporation of Amine and Polyamine Functional Groups. *Inorg. Chem.* **2019**, *58*, 4540−4552.

(8) Paterson, B. M.; Donnelly, P. S. Copper complexes of bis(thiosemicarbazones): from chemotherapeutics to diagnostic and therapeutic radiopharmaceuticals. *Chem. Soc. Rev.* **2011**, *40*, 3005−3018.

(9) Taniuchi, H.; Fujibayashi, Y.; Okazawa, H.; Yonekura, Y.; Konishi, J.; Yokoyama, A. Cu-pyruvaldehyde-bis(N4-methylthiosemicarbazone) (Cu-PTSM), a metal complex with selective NADH-dependent reduction by complex I in brain mitochondria: a potential radiopharmaceutical for mitochondria-functional imaging with positron emission tomography (PET). *Biol. Pharm. Bull.* **1995**, *18*, 1126−1129.

(10) Xie, D.; King, T. L.; Banerjee, A.; Kohli, V.; Que, E. L. Exploiting Copper Redox for F-19 Magnetic Resonance-Based Detection of Cellular Hypoxia. *J. Am. Chem. Soc.* **2016**, *138*, 2937−2940.

(11) Anjum, R.; Palanimuthu, D.; Kalinowski, D. S.; Lewis, W.; Park, K. C.; Kovacevic, Z.; Khan, I. U.; Richardson, D. R. Synthesis, Characterization, and in Vitro Anticancer Activity of Copper and Zinc Bis(Thiosemicarbazone) Complexes. *Inorg. Chem.* **2019**, *58*, 13709−13723.

(12) Cater, M. A.; Pearson, H. B.; Wolyniec, K.; Klaver, P.; Bilandzic, M.; Paterson, B. M.; Bush, A. I.; Humbert, P. O.; La Fontaine, S.; Donnelly, P. S.; Haupt, Y. Increasing Intracellular Bioavailable Copper Selectively Targets Prostate Cancer Cells. *ACS Chem. Biol.* **2013**, *8*, 1621−1631.

(13) Chandra, S.; Raizada, S.; Tyagi, M.; Gautam, A. Synthesis, spectroscopic, and antimicrobial studies on bivalent nickel and copper complexes of bis(thiosemicrbazone). *Bioinorg. Chem. Appl.* **2007**, *2007*, 51483.

(14) Dalecki, A. G.; Crawford, C. L.; Wolschendorf, F. Copper and Antibiotics: Discovery, Modes of Action, and Opportunities for Medicinal Applications. *Adv. Microb. Physiol.* **2017**, *70*, 193−260.

(15) Denoyer, D.; Clatworthy, S. A. S.; Cater, M. A., Copper Complexes in Cancer Therapy. *Met. Ions. Life. Sci.* **2018**.469

(16) Hung, L. W.; Villemagne, V. L.; Cheng, L.; Sherratt, N. A.; Ayton, S.; White, A. R.; Crouch, P. J.; Lim, S.; Leong, S. L.; Wilkins, S.; George, J.; Roberts, B. R.; Pham, C. L. L.; Liu, X.; Chiu, F. C. K.; Shackleford, D. M.; Powell, A. K.; Masters, C. L.; Bush, A. I.; O'Keefe, G.; Culvenor, J. G.; Cappai, R.; Cherny, R. A.; Donnelly, P. S.; Hill, A. F.; Finkelstein, D. I.; Barnham, K. J. The hypoxia imaging agent Cu-II(atsm) is neuroprotective and improves motor and cognitive functions in multiple animal models of Parkinson's disease. *J. Exp. Med.* **2012**, *209*, 837−854.

(17) Collaborative Medicinal Development Pty Limited. *Phase 1 Dose Escalation and PK Study of Cu(II)ATSM in ALS/MND*. https://clinicaltrials.gov/ct2/show/NCT02870634, 2016.

(18) Palanimuthu, D.; Shinde, S. V.; Somasundaram, K.; Samuelson, A. G. In Vitro and in Vivo Anticancer Activity of Copper Bis(thiosemicarbazone) Complexes. *J. Med. Chem.* **2013**, *56*, 722−734.

https://dx.doi.org/10.1021/acs.inorgchem.0c00182
Inorg. Chem. XXXX, XXX, XXX−XXX

(19) Palma, E.; Mendes, F.; Morais, G. R.; Rodrigues, I.; Santos, I. C.; Campello, M. P. C.; Raposinho, P.; Correia, I.; Gama, S.; Belo, D.; Alves, V.; Abrunhosa, A. J.; Santos, I.; Paulo, A. Biophysical characterization and antineoplastic activity of new bis-(thiosemicarbazonato) Cu(II) complexes. *J. Inorg. Biochem.* **2017**, *167*, 68−79.
(20) Roberts, B. R.; Lim, N. K. H.; McAllum, E. J.; Donnelly, P. S.; Hare, D. J.; Doble, P. A.; Turner, B. J.; Price, K. A.; Lim, S. C.; Paterson, B. M.; Hickey, J. L.; Rhoads, T. W.; Williams, J. R.; Kanninen, K. M.; Hung, L. W.; Liddell, J. R.; Grubman, A.; Monty, J. F.; Llanos, R. M.; Kramer, D. R.; Mercer, J. F. B.; Bush, A. I.; Masters, C. L.; Duce, J. A.; Li, Q. X.; Beckman, J. S.; Barnham, K. J.; White, A. R.; Crouch, P. J. Oral Treatment with Cu-II(atsm) Increases Mutant SOD1 In Vivo but Protects Motor Neurons and Improves the Phenotype of a Transgenic Mouse Model of Amyotrophic Lateral Sclerosis. *J. Neurosci.* **2014**, *34*, 8021−8031.
(21) French, F. A.; Freedlander, B. L. Carcinostatic action of polycarbonyl compounds and their derivatives. IV. Glyoxal bis (thiosemicarbazone) and derivatives. *Cancer Res.* **1958**, *11*, 1290−300.
(22) Booth, B. A.; Sartorelli, A. C. Synergistic interaction of kethoxal bis(thiosemicarbazone) and cupric ions in sarcoma 180. *Nature* **1966**, *210*, 104−105.
(23) Mihich, E.; Nichol, C. A. Kethoxal bis(thiosemicarbazone). I. Effects against experimental tumors. *Cancer Res.* **1965**, *25* (9), 1410−1416.
(24) Petering, H. G.; Buskirk, H. H.; Underwood, G. E. The Anti-Tumor Activity of 2-Keto-3-Ethoxybutyraldehyde Bis-(Thiosemicarbazone) and Related Compounds. *Cancer Res.* **1964**, *24* (3), 367−372.
(25) Cappuccino, J. G.; Banks, S.; Brown, G.; George, M.; Tarnowski, G. S. The effect of copper and other metal ions on the antitumor activity of pyruvaldehyde bis(thiosemicarbazone). *Cancer Res.* **1967**, *27* (5), 968−973.
(26) Minkel, D. T.; Petering, D. H. Initial Reaction of 3-Ethoxy-2-Oxobutyraldehyde Bis(Thiosemicarbazonato) Copper(II) with Ehrlich Ascites Tumor-Cells. *Cancer Res.* **1978**, *38* (1), 117−123.
(27) Minkel, D. T.; Saryan, L. A.; Petering, D. H. Structure-Function Correlations in Reaction of Bis(Thiosemicarbazonato) Copper(II) Complexes with Ehrlich Ascites Tumor-Cells. *Cancer Res.* **1978**, *38* (1), 124−129.
(28) Petering, H. G.; Buskirk, H. H.; Crim, J. A. The effect of dietary mineral supplements of the rat on the antitumor activity of 3-ethoxy-2-oxobutyraldehyde bis(thiosemicarbazone). *Cancer Res.* **1967**, *27* (6), 1115−1121.
(29) Djoko, K. Y.; Goytia, M. M.; Donnelly, P. S.; Schembri, M. A.; Shafer, W. M.; McEwan, A. G. Copper(II)-Bis(Thiosemicarbazonato) Complexes as Antibacterial Agents: Insights into Their Mode of Action and Potential as Therapeutics. *Antimicrob. Agents Chemother.* **2015**, *59* (10), 6444−6453.
(30) Haeili, M.; Moore, C.; Davis, C. J.; Cochran, J. B.; Shah, S.; Shrestha, T. B.; Zhang, Y.; Bossmann, S. H.; Benjamin, W. H.; Kutsch, O.; Wolschendorf, F. Copper complexation screen reveals compounds with potent antibiotic properties against methicillin-resistant Staphylococcus aureus. *Antimicrob. Agents Chemother.* **2014**, *58* (7), 3727−3736.
(31) Bandara, N.; Sharma, A. K.; Krieger, S.; Schultz, J. W.; Han, B. H.; Rogers, B. E.; Mirica, L. M. Evaluation of (64)Cu-Based Radiopharmaceuticals that Target Abeta Peptide Aggregates as Diagnostic Tools for Alzheimer's Disease. *J. Am. Chem. Soc.* **2017**, *139* (36), 12550−12558.
(32) Hickey, J. L.; Lim, S.; Hayne, D. J.; Paterson, B. M.; White, J. M.; Villemagne, V. L.; Roselt, P.; Binns, D.; Cullinane, C.; Jeffery, C. M.; Price, R. I.; Barnham, K. J.; Donnelly, P. S. Diagnostic Imaging Agents for Alzheimer's Disease: Copper Radiopharmaceuticals that Target A beta Plaques. *J. Am. Chem. Soc.* **2013**, *135* (43), 16120−16132.
(33) Santini, C.; Pellei, M.; Gandin, V.; Porchia, M.; Tisato, F.; Marzano, C. Advances in copper complexes as anticancer agents. *Chem. Rev.* **2014**, *114* (1), 815−862.
(34) Santoro, A.; Vileno, B.; Palacios, O.; Peris-Diaz, M. D.; Riegel, G.; Gaiddon, C.; Krezel, A.; Faller, P. Reactivity of Cu(II)-, Zn(II)- and Fe(II)-thiosemicarbazone complexes with glutathione and metallothionein: from stability to dissociation to transmetallation. *Metallomics* **2019**, *11* (5), 994−1004.
(35) Wehbe, M.; Leung, A. W. Y.; Abrams, M. J.; Orvig, C.; Bally, M. B. A Perspective - can copper complexes be developed as a novel class of therapeutics? *Dalton Trans.* **2017**, *46* (33), 10758−10773.
(36) Skrott, Z.; Mistrik, M.; Andersen, K. K.; Friis, S.; Majera, D.; Gursky, J.; Ozdian, T.; Bartkova, J.; Turi, Z.; Moudry, P.; Kraus, M.; Michalova, M.; Vaclavkova, J.; Dzubak, P.; Vrobel, I.; Pouckova, P.; Sedlacek, J.; Miklovicova, A.; Kutt, A.; Li, J.; Mattova, J.; Driessen, C.; Dou, Q. P.; Olsen, J.; Hajduch, M.; Cvek, B.; Deshaies, R. J.; Bartek, J. Alcohol-abuse drug disulfiram targets cancer via p97 segregase adaptor NPL4. *Nature* **2017**, *552* (7684), 194−199.
(37) Tsvetkov, P.; Detappe, A.; Cai, K.; Keys, H. R.; Brune, Z.; Ying, W.; Thiru, P.; Reidy, M.; Kugener, G.; Rossen, J.; Kocak, M.; Kory, N.; Tsherniak, A.; Santagata, S.; Whitesell, L.; Ghobrial, I. M.; Markley, J. L.; Lindquist, S.; Golub, T. R. Mitochondrial metabolism promotes adaptation to proteotoxic stress. *Nat. Chem. Biol.* **2019**, *15* (7), 681−689.
(38) Vishnosky, N. S.; Mashuta, M. S.; Buchanan, R. M.; Grapperhaus, C. A. Syntheses, structures, and electrochemical studies of N, N '-bis (alkylthiocarbamate) butane-2,3-diimine Cu(II) complexes as pendent alkoxy derivatives of Cu(ATSM). *Inorg. Chim. Acta* **2017**, *461*, 45−51.
(39) Rufenacht, K. Arbetien über Phosphosäure- und Thiosphosphorsäureester mit einem Heterocyclischen Substituenten Thiadiazol-Ringschluss und eine Dabei Auftretende Methylübertragung. *Helv. Chim. Acta* **1972**, *55*, 1178−1187.
(40) Gingras, B. A.; Suprunchuk, T.; Bayley, C. H. The Preparation of Some Thiosemicarbazones and Their Copper Complexes: Part III. *Can. J. Chem.* **1962**, *40* (6), 1053−1059.
(41) *CrysAlis PRO RED: SCALE3 ABSPACK*, Ver. 1.171.36.32; Agilent Technologies: Oxfordshire, England, 2013.
(42) Bazhenova, T. A.; Shilov, A. E. Nitrogen-Fixation in Solution. *Coord. Chem. Rev.* **1995**, *144*, 69−145.
(43) Sheldrick, G. M. A short history of SHELX. *Acta Crystallogr., Sect. A: Found. Crystallogr.* **2008**, *64*, 112−122.
(44) Bates, P. J.; Kahlon, J. B.; Thomas, S. D.; Trent, J. O.; Miller, D. M. Antiproliferative activity of G-rich oligonucleotides correlates with protein binding. *J. Biol. Chem.* **1999**, *274* (37), 26369−26377.
(45) Salipur, F. R.; Reyes-Reyes, E. M.; Xu, B.; Hammond, G. B.; Bates, P. J. A novel small molecule that induces oxidative stress and selectively kills malignant cells. *Free Radical Biol. Med.* **2014**, *68*, 110−121.
(46) Guzman, C.; Bagga, M.; Kaur, A.; Westermarck, J.; Abankwa, D. ColonyArea: an ImageJ plugin to automatically quantify colony formation in clonogenic assays. *PLoS One* **2014**, *9*, No. e92444.
(47) West, D. X.; Ives, J. S.; Bain, G. A.; Liberta, A. E.; ValdesMartinez, J.; Ebert, K. H.; HernandezOrtega, S. Copper(II) and nickel(II) complexes of 2,3-butanedione bis(N(3)-substituted thiosemicarbazones). *Polyhedron* **1997**, *16*, 1895−1905.
(48) Farrugia, L. ORTEP-3 for Windows - a version of ORTEP-III with a Graphical User Interface (GUI). *J. Appl. Crystallogr.* **1997**, *30*, 565.
(49) Blower, P. J.; Castle, T. C.; Cowley, A. R.; Dilworth, J. R.; Donnelly, P. S.; Labisbal, E.; Sowrey, F. E.; Teat, S. J.; Went, M. J. Structural trends in copper(II) bis(thiosemicarbazone) radiopharmaceuticals. *Dalton Trans.* **2003**, *23*, 4416−4425.
(50) Jain, R.; Al Mamun, A.; Buchanan, R. M.; Kozlowski, P. M.; Grapperhaus, C. A. Ligand-Assisted Metal-Centered Electrocatalytic Hydrogen Evolution upon Reduction of a Bis(thiosemicarbazonato)-Ni(II) Complex. *Inorg. Chem.* **2018**, *57*, 13486−13493.
(51) Spek, A. L. Structure validation in chemical crystallography. *Acta Crystallogr., Sect. D: Biol. Crystallogr.* **2009**, *65*, 148−155.

https://dx.doi.org/10.1021/acs.inorgchem.0c00182
Inorg. Chem. XXXX, XXX, XXX−XXX

(52) Kenche, V. B.; Barnham, K. J. Alzheimer's disease & metals: therapeutic opportunities. *Br. J. Pharmacol.* **2011**, *163*, 211−219.
(53) McAllum, E. J.; Roberts, B. R.; Hickey, J. L.; Dang, T. N.; Grubman, A.; Donnelly, P. S.; Liddell, J. R.; White, A. R.; Crouch, P. J. Zn-II(atsm) is protective in amyotrophic lateral sclerosis model mice via a copper delivery mechanism. *Neurobiol. Dis.* **2015**, *81*, 20−24.
(54) Vavere, A. L.; Lewis, J. S. Cu-ATSM: A radiopharmaceutical for the PET imaging of hypoxia. *Dalton Trans.* **2007**, *43*, 4893−4902.
(55) Haddad, A. Z.; Garabato, B. D.; Kozlowski, P. M.; Buchanan, R. M.; Grapperhaus, C. A. Beyond Metal-Hydrides: Non-Transition-Metal and Metal-Free Ligand-Centered Electrocatalytic Hydrogen Evolution and Hydrogen Oxidation. *J. Am. Chem. Soc.* **2016**, *138*, 7844−7847.
(56) Holland, J. P.; Aigbirhio, F. I.; Betts, H. M.; Bonnitcha, P. D.; Burke, P.; Christlieb, M.; Churchill, G. C.; Cowley, A. R.; Dilworth, J. R.; Donnelly, P. S.; Green, J. C.; Peach, J. M.; Vasudevan, S. R.; Warren, J. E. Functionalized Bis(thiosemicarbazonato) Complexes of Zinc and Copper: Synthetic Platforms Toward Site-Specific Radiopharmaceuticals. *Inorg. Chem.* **2007**, *46*, 465−485.
(57) Matsumoto, K.; Fujibayashi, Y.; Arano, Y.; Wada, K.; Yokoyama, A. 62Cu-labeled bifunctional radiopharmaceuticals with metabolizable ester groups. *Int. J. Rad. Appl. Instrum. B* **1992**, *19*, 33−38.
(58) Saji, H. Synthesis and in vivo behavior of a copper64labeled dithiosemicarbazone derivative coupled to a dihydropyridine carrier. *J. Labelled Compd. Radiopharm.* **1993**, *33*, 127.
(59) Shoemaker, R. H. The NCI 60 human tumor cell line screen: An information-rich screen informing on mechanisms of toxicity. *Nat. Rev. Cancer* **2006**, *6*, 813−823.
(60) Ahmad, M.; Suhaimi, S. N.; Chu, T. L.; Aziz, N. A.; Kornain, N. K. M.; Samiulla, D. S.; Lo, K. W.; Ng, C. H.; Khoo, A. S. B., Ternary copper(II) complex: NCI60 screening, toxicity studies, and evaluation of efficacy in xenograft models of nasopharyngeal carcinoma. *PLoS One* **2018**, *13*.e0191295
(61) Slator, C.; Barron, N.; Howe, O.; Kelleet, A. [Cu(o-phthalate)(phenanthroline)] Exhibits Unique Superoxide-Mediated NCI-60 Chemotherapeutic Action through Genomic DNA Damage and Mitochondrial Dysfunction. *ACS Chem. Biol.* **2016**, *11*, 159−171.
(62) Slator, C.; Molphy, Z.; Mckee, V.; Long, C.; Brown, T.; Kellett, A. Di-copper metallodrugs promote NCI-60 chemotherapy via singlet oxygen and superoxide production with tandem TA/TA and AT/AT oligonucleotide discrimination. *Nucleic Acids Res.* **2018**, *46*, 2733−2750.
(63) Stacy, A. E.; Palanimuthu, D.; Bernhardt, P. V.; Kalinowski, D. S.; Jansson, P. J.; Richardson, D. R. Zinc(II)-Thiosemicarbazone Complexes Are Localized to the Lysosomal Compartment Where They Transmetallate with Copper Ions to Induce Cytotoxicity. *J. Med. Chem.* **2016**, *59*, 4965−4984.

https://dx.doi.org/10.1021/acs.inorgchem.0c00182
Inorg. Chem. XXXX, XXX, XXX−XXX